Applied Catalysis B: Environmental 238 (2018) 586–591

Contents lists available at ScienceDirect

Applied Catalysis B: Environmental

journal homepage: www.elsevier.com/locate/apcatb

Fabrication of $BiVO_4$ photoanode consisted of mesoporous nanoparticles with improved bulk charge separation efficiency

Haipeng Zhang[a], Huiliang Li[a], Zeyan Wang[a,*], Zhaoke Zheng[a], Peng Wang[a], Yuanyuan Liu[a], Xiaoyang Zhang[a], Xiaoyan Qin[a], Ying Dai[b], Baibiao Huang[a,*]

[a] State Key Laboratory of Crystal Materials, Shandong University, China
[b] School of Physics, Shandong University, China

ARTICLE INFO

Keywords:
Mesoporous $BiVO_4$
Photoelectrochemical water splitting
Bulk charge separation

ABSTRACT

In this work, we developed a simple method to fabricate $BiVO_4$ photoanode consisted of mesoporous nanoparticles (meso-BVO) by using P123 as a pore maker. Owing to the unique mesoporous nanostructure, meso-BVO exhibits higher BET surface areas, shorter hole transit distance and higher electrical conductivity than does pristine $BiVO_4$ photoanode (BVO) consisted of solid nanoparticles. As a result, the charge separation efficiency and PEC performances of meso-BVO have been greatly improved. Meso-BVO yields a photocurrent of 2.19 mA/cm^2 (1.23 V vs RHE) and IPCE of 39% (420 nm), which is 2.52 and 2 times as high as that of pristine BVO. With the assistance of Mo^{6+} ions doping and Co-Pi, the PEC performances could be further improved by addressing the inefficient electron transport and slow water oxidation kinetics. Co-Pi/Mo:meso-BVO yields a photocurrent of 4.57 mA/cm^2 (1.23 V vs RHE) and IPCE value of 65% (420 nm). The enhanced PEC performance can be mainly ascribed to the perfect charge separation in the bulk of Co-Pi/Mo:meso-BVO photoanode. Our work provides a simple method to fabricate high efficient $BiVO_4$ photoanodes consisted of mesoporous nanoparticles with enhanced bulk charge separation efficiencies.

1. Introduction

Photoelectrochemical (PEC) water splitting to produce hydrogen and oxygen under solar light irradiation is regarded as one of the most promising strategy to solve the energy and environmental crisis owing to its high theoretical conversion efficiencies and low cost [1–7]. Among those available semiconductors, monoclinic $BiVO_4$, with a direct band gap of ~2.4 eV, emerges as one of the most attractive candidate to fabricate high efficient PEC photoanode with visible light responses, with a theoretical maximum photocurrent density of 7.5 mA/cm^2 and solar-to-hydrogen (STH) conversion efficiency of ~9.1% under AM 1.5 G irradiation [8–10]. However, limited by the poor electrical conductivity, short carrier diffusion length, and slow oxidation kinetics, the PEC performance of $BiVO_4$ photoanode is still far below the maximum attainable [11–13]. To date, various strategies have been developed to address these issues, such as doping of Mo^{6+} or W^{6+} ions to improve the conductivity [13–16], construction of hetero-/homo-junctions to promote the charge separation [17–19], loading of oxygen evolution catalysts to accelerate the surface oxidation kinetics and improve the stability of $BiVO_4$ photoanodes, etc [20–24]. Unfortunately, the poor charge separation efficiency ascribed from the short hole diffusion length could be still a remaining problem that limiting the PEC performance of $BiVO_4$ photoanodes [12,16,25–27].

The hole diffusion length (L_P) in $BiVO_4$ is reported to be 70–200 nm [24,28–30]. For efficient hole collection, the hole transit distance in $BiVO_4$ films should be shorter than L_P. Thus, nanoporous $BiVO_4$ structures consisted of nanoparticles smaller than 100 nm have been fabricated recently to enhance the charge separation by shortening the hole transit distance. However, the charge separation efficiency in these nanoporous $BiVO_4$ photoanode is still not satisfactory [15,16,31–33]. That could be probably attributed to the variable L_P in $BiVO_4$ films prepared by different procedures depending on their different crystallinity, bulk defects or surface properties [12,15]. For example, the L_P in nanoporous Mo:$BiVO_4$ films reported by Li et al. is estimated to be only ~20 nm [34]. Therefore, L_P must be several times longer than the largest hole transit distance in $BiVO_4$ photoanode to guarantee satisfying hole collection efficiency. That means the particle size in $BiVO_4$ nanostructures should be as small as possible for efficient hole collections. However, on the other hand, the electron transport in these $BiVO_4$ nanostructures consisted of small nanoparticles could be

* Corresponding authors.
E-mail addresses: wangzeyan@sdu.edu.cn (Z. Wang), bbhuang@sdu.edu.cn (B. Huang).

https://doi.org/10.1016/j.apcatb.2018.07.050
Received 6 May 2018; Received in revised form 11 July 2018; Accepted 15 July 2018
Available online 17 July 2018
0926-3373/

hindered, because the electrons have to transit more grain boundaries, and are easily got recombined before reaching the back contact with the decrease on particle sizes. The conflict between particle size and long-range electronic connectivity make it still a great challenge to improve the charge separation efficiency of $BiVO_4$ photoanodes.

Recent success on the fabrication of mesoporous metal oxide single crystals could provide a possible route to address both the above problems [35,36]. With mesoscale pores in micro- or sub-micrometer-size particles, mesoporous single crystals not only provide larger accessible surface areas and short hole transit distance, but also exhibit enhanced long-range electron conductivity. Thus, both the criteria for efficient hole collections and electron transport could be satisfied in $BiVO_4$ photoanodes consisted of mesoporous single crystals, which is expected to exhibit enhanced charge separation efficiency and better PEC performances. Although this kind of photoanodes consisted of metal oxides mesoporous single crystalline nanoparticles, i.e., Fe_2O_3, TiO_2, have been reported [36,37], the fabrication of $BiVO_4$ photoanode consisted of mesoporous nanoparticles is still a challenge work, which has not been reported yet. Herein, we developed a simple method to fabricate $BiVO_4$ photoanode consisted of mesoporous nanoparticles (meso-BVO) by employing P123 as a pore maker. Owing to the unique mesoporous nanostructure, the charge separation efficiency and the PEC performance has been greatly improved.

2. Results and discussions

Meso-BVO was fabricated by spin-coating followed by subsequent annealing treatment with the addition of P123 in the precursor solution as described in Supporting Information. For comparison, pristine $BiVO_4$ photoanode (BVO) without P123 was also prepared following the identical procedure. The structures of as-prepared BVO and meso-BVO were characterized by X-ray diffractions (XRD). As shown in Fig. 1a, both of the XRD patterns of as-prepared BVO and meso-BVO can be indexed to monoclinic $BiVO_4$ (JPCDS No.14-688) besides few peaks corresponding to FTO substrate (marked with * in Fig. 1a). The average crystallite size calculated from Scherrer broadening of the primary (−121) peak for BVO and meso-BVO is 31.3 and 31.4 nm, respectively. The similar crystallite size in either BVO or meso-BVO indicates the addition of P123 has little effect on the crystallization in the as-prepared samples. The light absorption of as-prepared BVO and meso-BVO were measured by UV–vis spectrophotometer equipped with an integrating sphere. As shown in the diffused reflectance spectra in Fig. 1b, the absorption edge of pristine BVO and meso-BVO is almost identical. And the band gap of both BVO and meso-BVO was estimated to be 2.58 eV. This indicates the addition of P123 did not apparently affect the light absorption and band gap of $BiVO_4$ photoanode.

The morphologies of BVO and meso-BVO were characterized by SEM and HR-TEM as shown in Figs. S1 and 2 . The thickness of the as-prepared BVO and meso-BVO film is about 500 nm according to the cross-sectional SEM image as shown in the insets of Fig. S1. And the top-view SEM images indicate that the as-prepared BVO and meso-BVO are porous films consisted of aggregated nanoparticles with irregular shapes. Some pin-holes can be observed on the surface of both BVO and meso-BVO films, while the size of the pin-holes are different for BVO and meso-BVO. The size of the pin-holes on the surface of meso-BVO is ~50–200 nm, which is much larger than that on the surface of BVO (~20–100 nm). The larger pin-holes on the surface of meso-BVO film can be ascribed to the addition of P123, which could produce more gaseous products than does BVO during annealing treatment. The HR-TEM images taken from the fragments of the as-prepared BVO and meso-BVO films were shown in Fig. 2. It can be seen that both of BVO and meso-BVO are porous structures consisted of inter-connected nanoparticles. And the clear selected area electron diffraction (SAED) patterns as shown in the insets of Fig. 2a and b indicate the as-prepared BVO and meso-BVO are polycrystalline consisted of several single crystals with high crystallinity. Zoomed-in views of the selected areas in Fig. 2a and b are presented in Fig. 2c and d, respectively. These images show that the surface of nanoparticles in BVO solid with smooth surface, while numerous mesoscale pores, with sizes ranging from ~5 to 30 nm, are evenly distributed in the nanoparticles of meso-BVO. That means meso-BVO is consisted of mesoporous nanoparticles, which is different from the pristine BVO consisted of solid nanoparticles.

The direct benefits of the presence of meso-pores in meso-BVO is the increase on surface areas. As shown in the N_2 adsorption-desorption isotherms in Fig. S2, the BET surface area of meso-BVO is 13.142 m^2/g, which is about 8.66 times as that of pristine BVO (1.517 m^2/g). Larger accessible surface areas can provide more active sites on the surface of the electrode, which would accelerate the surface reactions during PEC water splitting [38]. Additionally, the presence of meso-pores in meso-BVO could greatly shorten the hole transit distance to reach the surface of the electrode. As the distance between adjacent pores in meso-BVO is mostly less than 10 nm, holes only have to transit several nanometers to reach the surface of the electrode, which is much shorter than the reported L_P values and even comparative with the thickness of surface depletion layers [15,28,31]. However, the holes have to travel much longer distance (~30–50 nm) before reaching the electrode surface in BVO. Both the larger surface areas and reduced hole transit distance ascribed to the presence of meso-pores in meso-BVO are advantageous for charge separation and surface reactions during PEC water splitting. Thus, meso-BVO consisted of mesoporous nanoparticles are expected to exhibit better performance than does BVO consisted of solid nanoparticles during PEC water splitting.

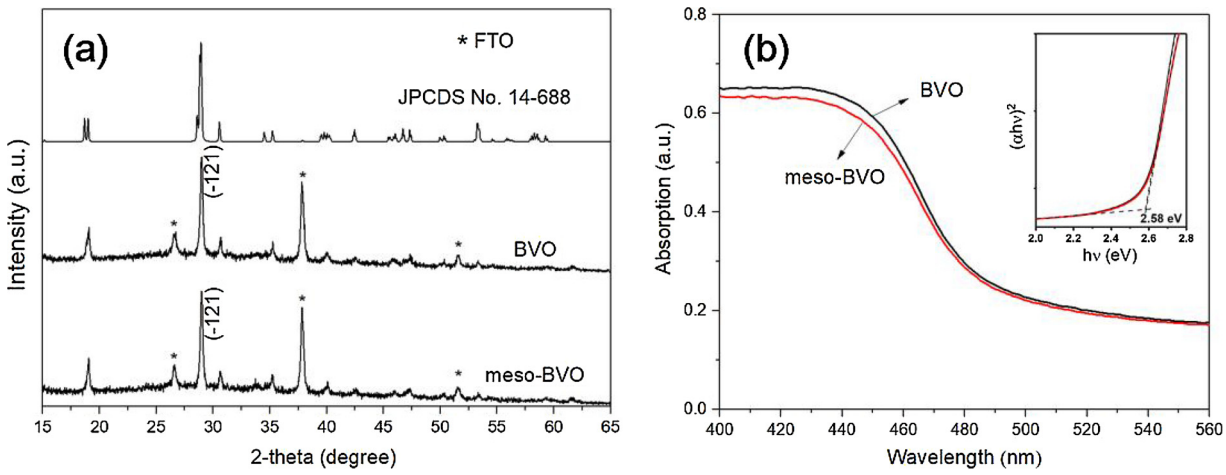

Fig. 1. (a) The XRD patterns and (b) diffused reflectance spectra of as-prepared BVO and meso-BVO. The inset of (b) shows the Tauc plots of BVO and meso-BVO.

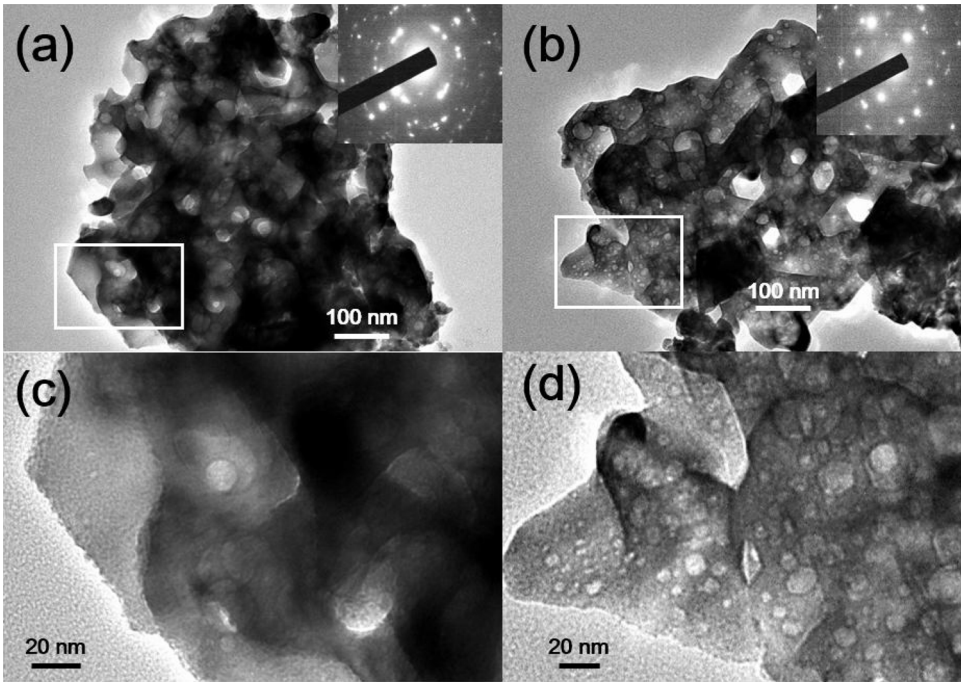

Fig. 2. HR-TEM images of as-prepared (a) BVO and (b) meso-BVO films. The insets of (a) and (b) shows the corresponding SAED patterns of BVO and meso-BVO. (c) and (d) shows the zoomed-in views of the selected areas in (a) and (b), respectively.

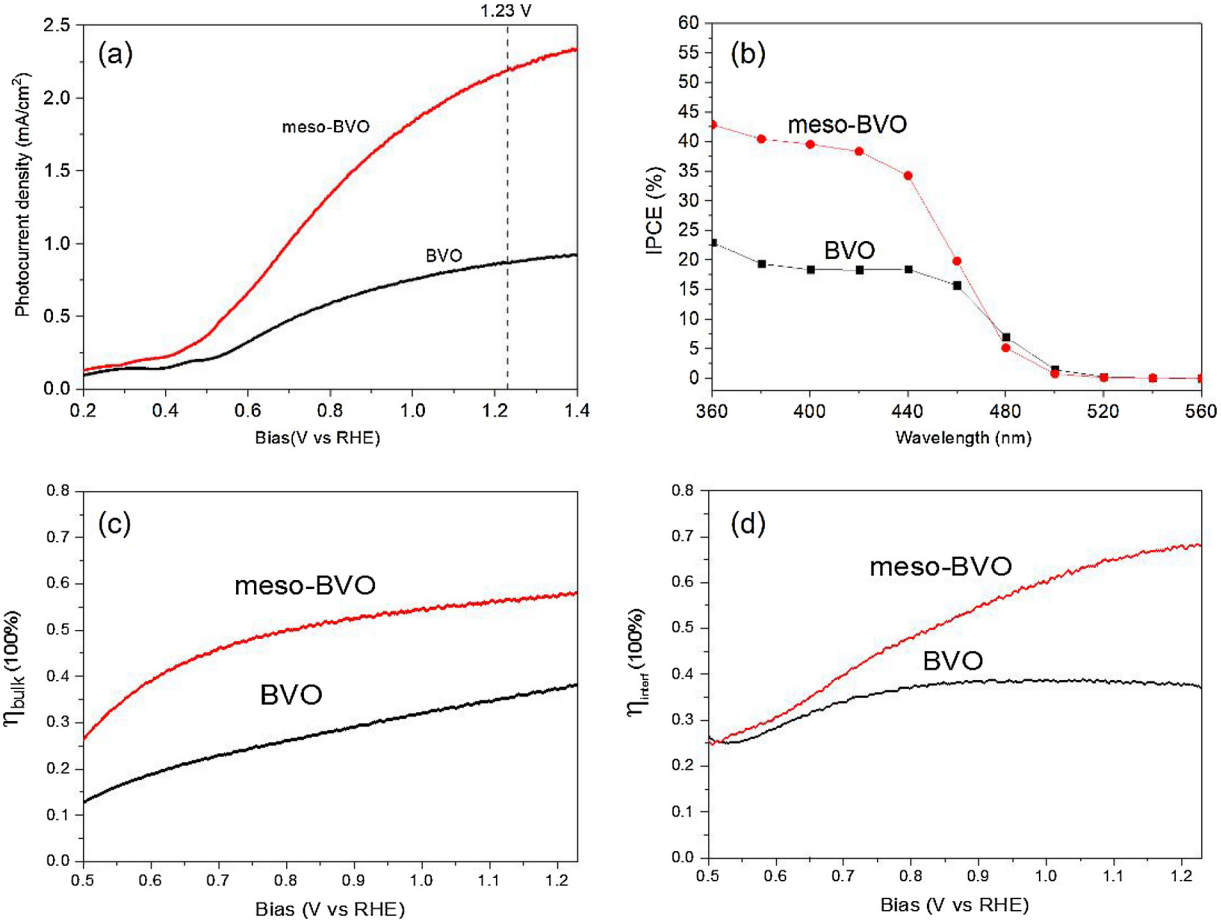

Fig. 3. (a) Photocurrent density versus applied potential curves (J-V) of as-prepared BVO and meso-BVO photoanodes with a scan rate of 10 mV/s under irradiation of AM 1.5 G simulated solar light (100 mW/cm^2) in 0.1 M potassium phosphate electrolyte solution (pH = 7). (b) The incident photon-to-current conversion efficiencies (IPCEs) of BVO and meso-BVO photoanodes measured at a bias of 1.23 V vs RHE. Charge separation efficiency (c) in the bulk (η_{bulk}) and (d) at the electrode/electrolyte interface (η_{interf}) in BVO and meso-BVO photoanodes.

To verifying the above assumption, the PEC performances of as-prepared BVO and meso-BVO were investigated by employing a three electrode configuration with as-prepared samples as the working electrode, a Pt sheet as the counter electrode and saturated calomel electrode (SCE) as the reference electrode measured in 0.1 M potassium phosphate electrolyte (pH = 7) under AM 1.5 G simulated solar light (100 mW/cm^2). As shown in the J-V plots in Fig. 3a, pristine BVO photoanode yields a photocurrent density of 0.87 mA/cm^2 at 1.23 V vs RHE, which is comparative with the reported values. With the addition of P123, meso-BVO exhibits higher photocurrent density than that of BVO as expected. At the same bias, the photocurrent density of meso-BVO is measured to be 2.19 mA/cm^2, which is 2.52 times as high as that of pristine BVO. And this value is not only much larger than the reported photoanodes consisted of mesoporous TiO_2 or Fe_2O_3 single crystals (0.74 mA/cm^2 for mesoporous TiO_2 photoanode, and 0.61 mA/cm^2 for mesoporous Fe_2O_3 photoanode) [36,37], but also one of the highest value for pure $BiVO_4$ photoanodes without doping and modification of cocatalysts [12–24,28,31].

The incident photon-to-current conversion efficiencies (IPCEs) of BVO and meso-BVO were also measured as shown in Fig. 3b. At the wavelength of 420 nm, the IPCE value of meso-BVO is measured to be 39%, which is two times larger as that of pristine BVO (19%). As the IPCE values can be expressed as:

$$IPCE = \eta_{abs} \cdot \eta_{bulk} \cdot \eta_{interf}$$

Where η_{abs} is the absorbance of the photoanode, η_{bulk} and η_{interf} the charge separation efficiency in the bulk and at the electrode/electrolyte interface, respectively. As the absorbance of as-prepared BVO and meso-BVO is almost identical as shown in Fig. S3, the enhanced PEC performance of meso-BVO photoanode could be ascribed to the improved charge separation efficiency in the bulk (η_{bulk}) and at the electrode/electrolyte interface (η_{interf}).

The η_{bulk} and η_{interf} of BVO and meso-BVO photoanodes were calculated and presented in Fig. 4c and d, respectively. At a bias of 1.23 V vs RHE, the η_{bulk} and η_{interf} value in pristine is only 38.5% and 37.5%, respectively. However, both the bulk and interfacial charge separation efficiency has been greatly improved in meso-BVO, with a η_{bulk} and η_{interf} value of 57.1% and 67.5% at the same bias, respectively, which is 1.48 and 1.82 times as high as that of pristine BVO, respectively. The enhanced charge separation efficiencies in meso-BVO could be mainly ascribed to the unique mesoporous nanostructures. As mentioned above, comparing to pristine BVO consisted of solid nanoparticles, meso-BVO exhibit larger surface areas and shorter hole transit distance. Therefore, both the charge separation in the bulk and at the electrode/electrolyte interface could be promoted in meso-BVO than in pristine BVO. However, the larger enhancement on η_{bulk} than η_{interf}, indicating the unique mesoporous nanostructures contribute more to the bulk charge separation in the electrode.

Besides the larger surface areas and shorter hole transit distance in meso-BVO, it is reported that the electrical conductivity in the film consisted mesoporous metal oxide single crystals is also much higher than in nanocrystalline films [36,37]. To address this point, we carried out electrochemical impendence spectra (EIS) analysis in both BVO and meso-BVO photoanodes. EIS analyses were carried out at 0 V vs SCE under light irradiation, and the Nyquist plots of BVO and meso-BVO are presented in Fig. S4. As can be seen, meso-BVO exhibits a smaller semicircle than does pristine BVO, which indicates the charge transfer resistance (R_{CT}) in meso-BVO is smaller than in BVO. By fitting the Nyquist plots using the equivalent circuit shown in Fig. S4, the R_{CT} value for BVO and meso-BVO is estimated to be 6.9 and 4.6 kΩ, respectively. This is also accordant with the reported results that the electrical conductivity is higher in the films consisted of mesoporous single crystals than in nanocrystalline films [36,37]. Therefore, the higher charge separation efficiency in meso-BVO could be attributed to the synergistic effects of higher surface areas, reduced hole transit distance and enhanced electrical conductivity, which can all ascribed to the unique mesoporous nanostructures.

Although the photocurrent and charge separation efficiency in meso-BVO have been greatly improved with comparison to pristine BVO, it is still not satisfactory, which could be probably limited by the inefficient electron transport owing to the relatively thick $BiVO_4$ layers (~500 nm). To confirm this suspect, the photocurrents of BVO and meso-BVO were measured under front (from the electrolyte to electrode) and back (from the substrate to the electrode) illumination. As the transit distance for photogenerated electrons is shorter under back illumination, the photocurrent would be much higher than that under front illumination when electron transport in the electrode is inefficient [39–41]. As shown in the *J–V* plots measured under front and back illumination in Fig. S5, the photocurrent of either BVO or meso-BVO under back illumination is much higher than that under front illumination, indicating the inefficient electron transport in as-prepared BVO and meso-BVO photoanodes.

In order to further improve the PEC performances of meso-BVO, Mo doped meso-BVO (Mo:meso-BVO) was fabricated to further improve the donor density and electrical conductivity of the electrode [13–16]. Comparing to meso-BVO, the structures, morphologies and light absorption properties of Mo:meso-BVO are almost identical as shown in Fig. S6. In order to prove the doping of Mo^{6+} in meso-BVO, XPS characterization was carried out. As shown in Fig. S7, two characteristic peaks centered at 232.4 and 235.5 eV can be observed in Mo:meso-BVO, which can be assigned to the 3d5/2 and 3d3/2 signals of Mo^{6+}, suggesting that Mo cations are mainly present as Mo^{6+} in Mo:meso-BVO [12,14,14,15,16]. The donor density calculated from the Mott-Schottky plots for Mo:meso-BVO and meso-BVO is 4.93×10^{19} *vs* 2.04×10^{19} cm^{-3}, respectively. (Fig. S8) The higher donor density in Mo:meso-BVO with respect to meso-BVO indicates the effective doping of Mo^{6+} in Mo:meso-BVO. With higher donor density in Mo:meso-BVO, the R_{CT} is also greatly reduced with comparison to meso-BVO. As shown in the Nyquist plots in Fig. S4, the R_{CT} value for Mo:meso-BVO is only 1.1 kΩ, which is only 23.6% of that in meso-BVO (4.6 kΩ). The PEC performance of Mo:meso-BVO was also investigated at the same conditions as described above. As shown in the J-V plots in Fig. 4a, the photocurrent of Mo:meso-BVO reaches 3.19 mA/cm^2 under 1.23 V vs RHE, which is 1.45 times as that of meso-BVO (2.19 mA/cm^2). Additionally, by changing the directions of illumination, the photocurrents are almost kept unchanged as shown in Fig. S9. That means the poor electron transport in meso-BVO has been well addressed in Mo:meso-BVO. To further improve the PEC performance of Mo:meso-BVO, Co-Pi was employed as a cocatalyst and loaded on the surface of Mo:meso-BVO to make Co-Pi/Mo:meso-BVO photoanode. According to the EDS spectrum in Fig. S10, both Co and P can be detected in Co-Pi/Mo:meso-BVO confirming the successful modification of Co-Pi on the surface of Mo:meso-BVO. After the modification of Co-Pi as cocatalysts, the photocurrent of Co-Pi/Mo:meso-BVO can be further improved to 4.57 mA/cm^2 at the same bias, which is two times larger than that of meso-BVO. The enhanced photocurrent in Co-Pi/Mo:meso-BVO can be attributed to the accelerated surface oxidation kinetics with the assistance of Co-Pi, because the donor density and the R_{CT} values of Co-Pi/Mo:meso-BVO photoanode are almost the same as that of Mo:meso-BVO photoanode as shown in the Nyquist and Mott-Schottky plots Figs. S4 and S8.

The stability of as-prepared Co-Pi/Mo:meso-BVO was investigated by sulfite and water oxidation under AM 1.5 G illumination at 1.23 V vs RHE. As shown in Fig. S11, Co-Pi/Mo:meso-BVO is quite stable in sulfite electrolyte solution with photocurrent kept almost unchanged after 2 h of continuous irradiation. However, the stability of Co-Pi/Mo:meso-BVO during water oxidation is much worse than for sulfite oxidation, with ~40% decrease on photocurrent after only 0.5 h of biased illumination, followed by a much slower decrease on photocurrent over the next 1.5 h. The decrease on photocurrent during water oxidation have been commonly observed in $BiVO_4$ photoanodes, which could be attributed to the photoinduced corrosion during PEC water splitting [31].

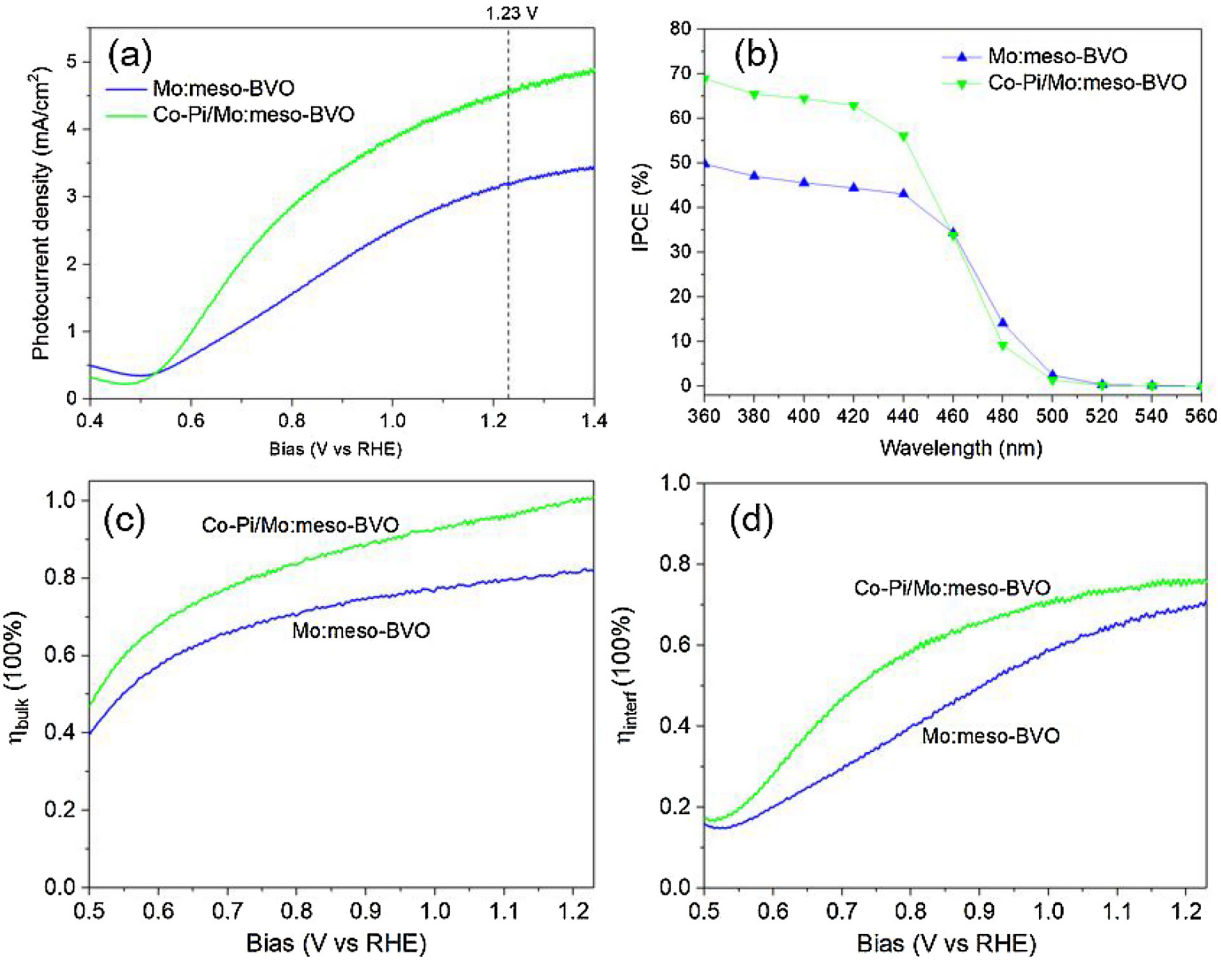

Fig. 4. (a) Photocurrent density versus applied potential curves (J-V) of Mo:meso-BVO and Co-Pi/Mo:meso-BVO photoanodes with a scan rate of 10 mV/s under irradiation of AM 1.5 G simulated solar light (100 mW/cm^2) in 0.1 M potassium phosphate electrolyte solution (pH = 7). (b) The IPCE curves of Mo:meso-BVO and Co-Pi/Mo:meso-BVO photoanodes measured at a bias of 1.23 V vs RHE. (c) η_{bulk} and (d) η_{interf} plots at different applied bias.

And this suggests the inhomogenous modification of Co-Pi on the accessible surface of the electrode owing to the mesoscale pore size in Mo:meso-BVO, which could be another issue to be addressed in the future.

Besides the enhancement on photocurrent, the conversion efficiencies of Mo:meso-BVO and Co-Pi/Mo:meso-BVO were also improved. As shown in the IPCE curve in Fig. 4b, the IPCE value for Mo:meso-BVO and Co-Pi/Mo:meso-BVO reaches 47% and 65%, respectively. The the η_{bulk} and η_{interf} plots of Mo:meso-BVO and Co-Pi/Mo:meso-BVO were also calculated as shown in Fig. 4c and d. The η_{bulk} and η_{interf} of Mo:meso-BVO at 1.23 V vs RHE is 82.1 and 70.5%, respectively. Comparing to that of meso-BVO, the η_{bulk} and η_{interf} of Mo:meso-BVO increase by 25 and 3%, respectively. This indicates the enhanced PEC performance of Mo:meso-BVO is mainly ascribed to the enhanced charge separation efficiency in the bulk. With the assistance of Co-Pi, both η_{bulk} and η_{interf} in Co-Pi/Mo:meso-BVO were further improved, with a η_{bulk} and η_{interf} of 99.8 and 76.5%, respectively. To be noticed, the η_{bulk} in Co-Pi/Mo:meso-BVO is close to unity, indicating perfect bulk charge separation in the electrode. However, the relative low η_{interf} value could be attributed to either inhomogenous modification of Co-Pi on electrode surface or poor interfaces between the electrode and cocatalysts.

Based on the above analysis, the charge separation process in BVO and meso-BVO can be illustrated as the schematic diagram in Fig. 5. During PEC water splitting, the electrons and holes, generated at the surface layer of the electrode under light irradiation, would move oppositely to the back contact and the surface of the electrode, respectively. In pristine BVO consisted of solid nanopartilces, the holes have to travel through the solid nanoparticles before reaching the electrode/electrolyte interface. While in meso-BVO, the distance that holes have to transit to reach the electrode/electrolyte interface would be greatly shortened owing to the presence of large amount of mesopores as illustrated in Fig. 5. Therefore, more holes would be able to escape from recombination before reaching the electrode surface in meso-BVO than in pristine BVO. Moreover, the electrical conductivity in meso-BVO is also improved comparing to BVO. Thus, meso-BVO consisted of mesoporous nanoparticles exhibits higher charge separation efficiency and higher photocurrent than does pristine BVO consisted of solid nanoparticles. However, limited by the relatively thick film and slow water oxidation kinetics, the charge separation efficiency in meso-BVO is still not satisfactory. To further improve the PEC performance, Mo^{6+} ions doping and Co-Pi loading were employed to address these issues. As expected, both the charge separation efficiency and PEC performance were further improved. And surprisingly, the bulk charge separation efficiency in Co-Pi/Mo:meso-BVO is almost 100%, which indicates the highly efficient charge separation in the as-prepared mesoporous $BiVO_4$ photoanode. Our results demonstrate the fabrication of $BiVO_4$ photoanode consisted of mesoporous nanoparticles could be an efficient strategy to promote the bulk charge separation by addressing its short hole diffusion lengths.

3. Conclusions

In this work, we fabricated meso-BVO consisted of mesoporous

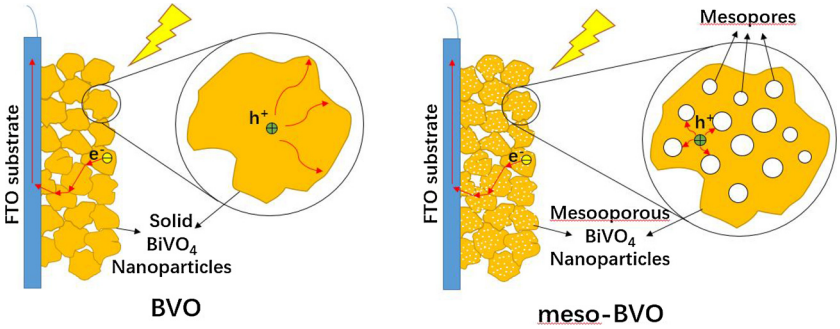

Fig. 5. Schematic diagram to illustrate the charge separation process in BVO and meso-BVO photoanodes.

nanoparticles with the assistance of P123 as a pore maker. Beneficial from the unique mesoporous nanostructure, meso-BVO exhibits larger BET surface areas, higher electrical conductivity and shorter hole transit distance comparing to pristine BVO consisted of solid nanoparticles. As a result, both the charge separation efficiency and the PEC performance in meso-BVO has been greatly improved. Meso-BVO yields a photocurrent of 2.2 mA/cm^2 at 1.23 V vs RHE and an IPCE value of 39% at 420 nm, which is 2.52 and 2 times as high as that of pristine BVO photoanode. With the assistance of Mo^{6+} ions doping and the modification of Co-Pi as a cocatalyst, the inefficient electron transport and slow water oxidation kinetics in meso-BVO can be well addressed. And Co-Pi/Mo:meso-BVO yields the highest photocurrent density of 4.57 mA/cm^2 at 1.23 V vs RHE, and IPCE value of 65% at 420 nm. According to the analyses on η_{bulk} and η_{interf}, the better PEC performance could be mainly ascribed to the enhanced charge separation in the bulk. The η_{bulk} of Co-Pi/Mo:meso-BVO at 1.23 V is almost 100%, indicating the efficient bulk charge separation in the electrode. Our work not only provide a simple method to fabricate $BiVO_4$ photoanode consisted of mesoporous nanoparticles, but also demonstrate it as an efficient method to improve the charge separation efficiency of $BiVO_4$ photoanode in the bulk.

Acknowlegements

This work is financially supported by the National Natural Science Foundation of China (21333006, 11374190, 21573135 and 51602179), the National Basic Research Program of China (the 973 Program, 2013CB632401). B.B.H. acknowledges the support from the Taishan Scholars Program of Shandong Province, and Z.Y.W. acknowledges the support from Young Scholars Program of Shandong University (2015WLJH35).

Appendix A. Supplementary data

Supplementary material related to this article can be found, in the online version, at doi:https://doi.org/10.1016/j.apcatb.2018.07.050.

References

[1] T. Bak, J. Nowotny, M. Rekas, C.C. Sorrell, Int. J. Hydrogen Energy 27 (2002) 991–1022.
[2] J.Z. Zhang, MRS Bull. 36 (2011) 48–55.
[3] H.L. Li, F.P. Li, Z.Y. Wang, Y.C. Jiao, Y.Y. Liu, P. Wang, X.Y. Zhang, X.Y. Qin, Y. Dai, B.B. Huang, Appl. Catal. B: Environ. 229 (2018) 114–120.
[4] Z.F. Liu, J. Zhang, W.G. Yan, ACS Sustain. Chem. Eng. 6 (2018) 3565–3574.
[5] X. Lu, Z.F. Liu, J.W. Li, J. Zhang, Z.G. Guo, Appl. Catal. B: Environ. 209 (2017) 657–662.
[6] T.T. Hong, Z.F. Liu, X.R. Zheng, J. Zhang, L. Yan, Appl. Catal. B: Environ. 202 (2017) 454–459.
[7] X.Z. Liang, P. Wang, M.M. Li, Q.Q. Zhang, Z.Y. Wang, Y. Dai, X.Y. Zhang, Y.Y. Liu, M. Whangbo, B.B. Huang, Appl. Catal., B 220 (2018) 356–361.
[8] A. Kudo, K. Omori, H. Kato, J. Am. Chem. Soc. 121 (1999) 11459–11467.
[9] H.W. Jeong, T.H. Jeon, J.S. Jang, W. Choi, H. Park, J. Phys. Chem. C 117 (2013) 9104–9112.
[10] Z.Y. Jiang, Y.Y. Liu, T. Jing, B.B. Huang, X.Y. Zhang, X.Y. Qin, Y. Dai, M.-H. Whangbo, J. Phys. Chem. C 120 (2016) 2058–2063.
[11] B. Zhang, H.P. Zhang, Z.Y. Wang, X.Y. Zhang, X.Y. Qin, Y. Dai, Y.Y. Liu, P. Wang, Y.J. Li, B.B. Huang, Appl. Catal., B 211 (2017) 258–265.
[12] Z.S. Li, W.J. Luo, M.L. Zhang, J.Y. Feng, Z.G. Zou, Energy Environ. Sci. 6 (2013) 347.
[13] Z.Y. Zhao, W.J. Luo, Z.S. Li, Z.G. Zou, Phys. Lett. A 374 (2010) 4919–4927.
[14] W.J. Luo, J.J. Wang, X. Zhao, Z.Y. Zhao, Z.S. Li, Z.G. Zou, Phys. Chem. Chem. Phys. 15 (2013) 1006.
[15] W.J. Luo, Z.S. Yang, Z.S. Li, J.Y. Zhang, J.G. Liu, Z.Y. Zhao, Z.Q. Wang, S.C. Yan, T. Yu, Z.G. Zou, Energy Environ. Sci. 4 (2011) 4046.
[16] J.A. Seabold, K. Zhu, N.R. Neale, Phys. Chem. Chem. Phys. 16 (2014) 1121.
[17] J.Z. Su, L.J. Guo, N.Z. Bao, C.A. Grimes, Nano Lett. 11 (2011) 1928–1933.
[18] J.S. Yang, J.J. Wu, Nano Energy 32 (2017) 232–240.
[19] Q.Z. Wang, J.J. Hea, Y.B. Shi, S.L. Zhang, T.J. Niua, H. Shea, Y.P. Bi, Z.Q. Lei, Appl. Catal., B 214 (2017) 158–167.
[20] B.B. Zhang, L. Wang, Y.J. Zhang, Y. Ding, Y.P. Bi, Angew. Chem. Int. Ed. 57 (2018) 2248–2252.
[21] M. Zhong, T. Hisatomi, Y. Kuang, J. Zhao, M. Liu, A. Iwase, Q.M. Jia, H. Nishiyama, T. Minegishi, M. Nakabayashi, N. Shibata, R. Niishiro, C. Katayama, H. Shibano, M. Katayama, A. Kudo, T. Yamada, K. Domen, J. Am. Chem. Soc. 137 (2015) 5053.
[22] J.Z. Su, L.J. Guo, N.Z. Bao, C.A. Grimes, Nano Lett. 11 (2011) 1928–1933.
[23] M.Z. Xie, X.D. Fu, L.Q. Jing, P. Luan, Y.J. Feng, H.G. Fu, L. Lived, Adv. Energy Mater. 4 (2014) 1300995.
[24] D.K. Zhong, S.J. Choi, D.R. Gamelin, J. Am. Chem. Soc. 133 (2011) 18370–18377.
[25] Y. Liu, Y.H. Guo, L.T. Schelhas, M. Li, J.W. Ager, J. Phys. Chem. C 120 (2016) 23449–23457.
[26] S.J.A. Moniz, J. Zhu, J. Tang, Adv. Energy Mater. 4 (2014) 1301590.
[27] M. Zhou, H.B. Wu, J. Bao, L.L, X.W. (David) Lou, Y. Xie, Angew. Chem. Int. Ed. 52 (2013) 8579–8583.
[28] F.F. Abdi, T.J. Savenije, M.M. May, B. Dam, R. van de Krol, J. Phys. Chem. Lett. 4 (2013) 2752–2757.
[29] G.W. Kim, G. Kang, J. Kim, G.Y. Lee, H. Kim, L. Pyeon, J. Lee, T. Park, Energy Environ. Sci. 7 (2014) 3424–3430.
[30] A.J.E. Rettie, H.C. Lee, L.G. Marshall, J.F. Lin, C. Capan, J. Lindemuth, J.S. McCloy, J.S. Zhou, A.J. Bard, C. Buddie Mullins, J. Am. Chem. Soc. 135 (2013) 11389–11396.
[31] V. Nair, C.L. Perkins, Q.Y. Lin, M. Law, Energy Environ. Sci. 9 (2016) 1412–1429.
[32] T.W. Kim, K.S. Choi, Science 13 (February) (2014) 1245026.
[33] C.C. Feng, Z.B. Jiao, S.P. Li, Y. Zhang, Y.B. Bi, Nanoscale 7 (2015) 20374–20379.
[34] X. Zhao, W. Luo, J. Feng, M. Li, Z. Li, T. Yu, Z. Zou, Adv. Energy Mater. 4 (2014) 1301785.
[35] E.J.W. Crossland, N. Noel, V. Sivaram, T. Leijtens, J.A. Alexander-Webber, H.J. Snaith, Nature 495 (2013) 215–219.
[36] C.W. Wang, S. Yang, W.Q. Fang, P. Liu, H.J. Zhao, H.G. Yang, Nano Lett. 16 (2016) 427–433.
[37] C. Zhen, T.T. Wu, M.W. Kadi, I. Ismail, G. Liu, H.M. Cheng, Chin. J. Catal. 36 (2015) 2171–2177.
[38] M. Zhou, J. Bao, Y. Xu, J.J. Zhang, J.F. Xie, M.L. Guan, C.L. Wang, L.Y. Wen, Y. Lei, Y. Xie, ACS Nano 8 (2014) 7088–7098.
[39] T.W. Kim, K.S. Choi, Science 343 (2014) 990–994.
[40] W.J. Luo, Z.S. Li, T. Yu†, Z.G. Zou, J. Phys. Chem. C 116 (2012) 5076–5081.
[41] Y.Q. Liang, T. Tsubota, L.P.A. Mooij, R.V.D. Krol, J. Phys. Chem. C 115 (35) (2011) 17594–17598.